Probabilistic Admissible Region for Short-Arc Angles-Only Observations

Islam I. Hussein and Christopher W. T. Roscoe
Applied Defense Solutions, Columbia, Maryland

Paul W. Schumacher, Jr.
Air Force Research Laboratory, Kihei, Hawaii

Matthew P. Wilkins
Applied Defense Solutions, Columbia, Maryland

ABSTRACT

The admissible region is defined as the set of physically acceptable orbits (i.e., orbits with negative energies). Given additional constraints on orbital semi-major axis, eccentricity, etc, the admissible region is further constrained, resulting in the constrained admissible region (CAR). Based on known statistics of the measurement process, in this paper we replace hard constraints with a probabilistic representation of the admissible region. This results in the probabilistic admissible region (PAR) that can be used for orbit initiation in Bayesian tracking. While this is a general concept that is applicable to any measurement scenario, we will illustrate the idea using a short-arc, angles-only observation scenario.

1. INTRODUCTION

As new optical sensors come online and more and more optical observations become available for space objects previously too small or too far away to detect, the space surveillance community is presented with the computationally challenging problem of generating initial orbit solutions for a large number of short-arc line-of-sight observations. In order to perform any kind of probability-based analysis with these orbit solutions, we require an accurate representation of their uncertainty. Properly characterizing the uncertainty will allow us to more efficiently deal with large sets of sparse data by enabling the use of rigorous probabilistic techniques to, for example, perform data association, determine collision probabilities, or initialize a Bayesian estimation scheme. This paper deals with the problem of characterizing uncertainty in a constrained admissible region (CAR) approach to initial orbit determination (IOD).

The admissible region approach has been previously used in the asteroid tracking community by Milani et al. [1, 2] to deal with the problem of identifying asteroids based on very short arc observations. Specifically, they referred to a region in the plane of possible ranges and range-rates defining those values for which a given line-of-sight observation produces an orbit solution that satisfies certain criteria. This concept has been extended in the SSA community by authors including Tommei [3, 4], Milani [5], Farnocchia [6], Rossi, Maruskin [7], Scheeres, Alfriend, Fujimoto [8, 9], Gronchi [10], Dimare, Schildknecht, Jehn, DeMars [11, 12], Jah, Schumacher, and Siminski [13, 14] to deal with the problem of tracking space objects in Earth orbit, for which the CAR refers to a region in the range, range-rate plane which produces orbit solutions with orbit elements satisfying some specified bounds. In previous work, Schumacher, Wilkins, and Roscoe [15,16] extended this concept to include regions in the range, range plane satisfying orbit element bounds for pairs of observations. Hussein et al. [17] applied probabilistic techniques to determining the admissibility of an uncertain candidate orbit in the CAR using both Unscented Transform (UT) and Monte Carlo (MC) methods. Worthy and Holzinger [18] incorporated measurement uncertainty into the admissible region approach for uncorrelated detections.

An unresolved topic in the SSA literature is how to best sample the CAR to perform data association or track initiation. For example, Tommei, Milani, and Rossi [3] use a Delaunay triangulation approach, while DeMars and Jah [12] (along with a number of other authors) use a uniform distribution approximated as a Gaussian Mixture Model (GMM). Simiski et al. [13, 14] use an Iso-Energy grid method to discretize the CAR along lines of equal energy (i.e., semi-major axis). The goal of the present work is to define a probabilistic form for the CAR to be used for initializing a Bayesian tracking scheme. Based on known statistics of the measurement process and assumed statistics in the semi-major axis and eccentricity, the probabilistic admissibility region (PAR) can be determined using a MC method. This resulting PAR which is made of a set of particles can then be converted to a GMM using the Expectation-Maximization (EM) algorithm [19, 20].

The paper is organized as follows. In Section 2., we review how the deterministic CAR is constructed. In Section 3., we describe how to construct the PAR from known measurement and RSO population statistics. In Section 4., we describe how to derive an MC representation of the PAR and in Section 5. we describe how to convert this particle cloud into a GMM using a versatile and robust EM algorithm called the FJ-EM algorithm. We provide a numerical example in Section 6. and conclude the paper in Section 7.

2. THE ANGLES-ONLY DETERMINISTIC CONSTRAINED ADMISSIBLE REGION

In this section we introduce the deterministic CAR for short-arc, angles-only optical observations. In the next section we introduce the PAR. The starting point is a series of n short-arc right ascension and declination observations (α_i, δ_i) taken at measurement times t_i, $i = 0, \ldots, n-1$, with epoch* at t_0. Following the second-order polynomial-in-time least squares procedure described by Maruskin, Scheeres, and Alfriend [7], one can obtain an estimate of the *optical attributable vector* $(\tilde{\alpha}_0, \dot{\tilde{\alpha}}_0, \tilde{\delta}_0, \dot{\tilde{\delta}}_0)$ at t_0 (we omit details here for brevity). For the rest of this paper we will drop the tilde and subscripts for ease of notation.

We now review how to construct the CAR from these estimates of the angles and their rates. We mostly follow the notation and derivation given by DeMars and Jah [12] (with minor corrections). Let $\mathbf{r}$ be the inertial position of the object, $\mathbf{q}$ be the inertial position of the ground station and $\boldsymbol{\rho}$ be the inertial position of the object with respect to the station. Hence, we have following position and velocity relationships

$$\mathbf{r} = \mathbf{q} + \boldsymbol{\rho} \tag{1}$$

and

$$\dot{\mathbf{r}} = \dot{\mathbf{q}} + \dot{\boldsymbol{\rho}}. \tag{2}$$

Using spherical coordinate system with respect to the ground station, $\boldsymbol{\rho}$ and its inertial time derivative can be expressed as

$$\boldsymbol{\rho} = \rho \mathbf{u}_\rho$$

$$\dot{\boldsymbol{\rho}} = \dot{\rho}\mathbf{u}_\rho + \rho\dot{\alpha}\cos\delta\mathbf{u}_\alpha + \rho\dot{\delta}\mathbf{u}_\delta, \tag{3}$$

where $\mathbf{u}_\rho$, $\mathbf{u}_\alpha$ and $\mathbf{u}_\delta$ are the spherical coordinate system's basis unit vectors and are given by

$$\begin{aligned}
\mathbf{u}_\rho &= (\cos\alpha\cos\delta, \sin\alpha\cos\delta, \sin\delta) \\
\mathbf{u}_\alpha &= (-\sin\alpha, \cos\alpha, 0) \\
\mathbf{u}_\delta &= (-\cos\alpha\sin\delta, -\sin\alpha\sin\delta, \cos\delta).
\end{aligned}$$

The position and velocity $\mathbf{r}$ and $\dot{\mathbf{r}}$ are related to the two-body energy via the equation

$$\mathcal{E} = \frac{\|\mathbf{r}\|^2}{2} - \frac{\mu}{\|\mathbf{r}\|} \tag{4}$$

After expressing $\mathbf{r}$ and $\dot{\mathbf{r}}$ in terms of the parameters $(\alpha, \dot{\alpha}, \delta, \dot{\delta}, \rho, \dot{\rho})$ this equation, it can be shown, is given by

$$\dot{\rho}^2 + w_1\dot{\rho} + F(\rho) - 2\mathcal{E} = 0 \tag{5}$$

where

$$F(\rho) = w_2\rho^2 + w_3\rho + w_4 - \frac{2\mu}{\sqrt{\rho^2 + w_5\rho + w_0}}$$

*Other epochs can be considered as well. For example, the mid-point of the arc may reduce error.

and where the parameters w_i ($i = 0, \ldots, 5$) are given by

$$
\begin{aligned}
w_0 &= \|\mathbf{q}\|^2 \\
w_1 &= 2\dot{\mathbf{q}} \cdot \mathbf{u}_\rho \\
w_2 &= \dot{\alpha}^2 \cos^2\delta + \dot{\delta}^2 \\
w_3 &= 2\dot{\alpha}\cos\delta(\dot{\mathbf{q}} \cdot \mathbf{u}_\alpha) + 2\dot{\delta}(\dot{\mathbf{q}} \cdot \mathbf{u}_\delta) \\
w_4 &= \|\dot{\mathbf{q}}\|^2 \\
w_5 &= 2\mathbf{q} \cdot \mathbf{u}_\rho
\end{aligned}
$$

Given a value for $\mathcal{E}$, one can solve for the corresponding curve in $\rho - \dot{\rho}$ space. The curve corresponding to $\mathcal{E} = 0$ defines the *admissible region* inside which all orbits with negative energy ($\mathcal{E} < 0$) exist. It is often the case, furthermore, that we have additional *inequality* constraints that one can impose in order to further limit the set of possible orbits with negative energy. Two important such constraints are constraints on semi-major axis, a, and eccentricity, e.

For the purpose of the discussion in the next section on the PAR, we will consider *equality* constraints on the semi-major axis and eccentricity. Given a fixed a, $\mathcal{E}$ in Eq. (5) can be replaced with

$$\mathcal{E} = -\frac{\mu}{2a} \tag{6}$$

resulting in

$$\dot{\rho}^2 + w_1\dot{\rho} + F(\rho) + \frac{\mu}{a} = 0. \tag{7}$$

Energy, is related to eccentricity (and orbital angular momentum) by [21]

$$\mathcal{E} = -\frac{\mu^2}{2\|\mathbf{h}\|^2}(1 - e^2). \tag{8}$$

However, note that the angular momentum $\mathbf{h}$ is related to the parameters $(\alpha, \dot{\alpha}, \delta, \dot{\delta}, \rho, \dot{\rho})$. One can show that $\mathbf{h}$ can be expressed as

$$\mathbf{h} = \mathbf{h}_1\dot{\rho} + \mathbf{h}_2\rho^2 + \mathbf{h}_3\rho + \mathbf{h}_4 \tag{9}$$

where (note that our expressions here differ from those of DeMars and Jah [12])

$$
\begin{aligned}
\mathbf{h}_1 &= \mathbf{q} \times \mathbf{u}_\rho \\
\mathbf{h}_2 &= \mathbf{u}_\rho \times (\dot{\alpha}\cos\delta\mathbf{u}_\alpha + \dot{\delta}\mathbf{u}_\delta) \\
\mathbf{h}_3 &= \mathbf{u}_\rho \times \dot{\mathbf{q}} + \mathbf{q} \times (\dot{\alpha}\cos\delta\mathbf{u}_\alpha + \dot{\delta}\mathbf{u}_\delta) \\
\mathbf{h}_4 &= \mathbf{q} \times \dot{\mathbf{q}}.
\end{aligned}
$$

Therefore, the magnitude squared of the angular momentum is given by

$$\|\mathbf{h}\|^2 = c_0\dot{\rho}^2 + P(\rho)\dot{\rho} + U(\rho), \tag{10}$$

where

$$
\begin{aligned}
P(\rho) &= c_1\rho^2 + c_2\rho + c_3 \\
U(\rho) &= c_4\rho^4 + c_5\rho^3 + c_6\rho^2 + c_7\rho + c_8,
\end{aligned}
$$

and where c_i ($i = 0, \ldots, 8$) are given by

$$
\begin{aligned}
c_0 &= \|\mathbf{h}_1\|^2 \\
c_1 &= 2\mathbf{h}_1 \cdot \mathbf{h}_2 \\
c_2 &= 2\mathbf{h}_1 \cdot \mathbf{h}_3 \\
c_3 &= 2\mathbf{h}_1 \cdot \mathbf{h}_4 \\
c_4 &= \|\mathbf{h}_2\|^2 \\
c_5 &= 2\mathbf{h}_2 \cdot \mathbf{h}_3 \\
c_6 &= 2\mathbf{h}_2 \cdot \mathbf{h}_4 + \|\mathbf{h}_3\|^2 \\
c_7 &= 2\mathbf{h}_3 \cdot \mathbf{h}_4 \\
c_8 &= \|\mathbf{h}_4\|^2
\end{aligned}
$$

Substituting Eq. (10) into Eq. (8), which in turn gets substituted into Eq. (5), one obtains

$$a_4\dot{\rho}^4 + a_3\dot{\rho}^3 + a_2\dot{\rho}^2 + a_1\dot{\rho} + a_0 = 0, \tag{11}$$

where a_i ($i = 0, \ldots, 4$) are functions of ρ and e and are given by:

$$
\begin{aligned}
a_0 &= F(\rho)U(\rho) + \mu^2(1 - e^2) \\
a_1 &= F(\rho)P(\rho) + w_1U(\rho) \\
a_2 &= U(\rho) + c_0F(\rho) + w_1P(\rho) \\
a_3 &= P(\rho) + c_0w_1 \\
a_4 &= c_0.
\end{aligned}
$$

For given values of a and e, in addition to the attributable variables $(\alpha, \dot{\alpha}, \delta, \dot{\delta})$ one can then solve the two nonlinear equations Eq. (7) and Eq. (11) for the unknowns ρ and $\dot{\rho}$. It is doubtful, however, that there exists a closed form solution to these equations.

3. PROBABILISTIC ADMISSIBLE REGION

The general goal is to obtain the probabilistic characterization of the uncertainty in the variables $(\rho, \dot{\rho})$ given knowledge of the statistics of the angles-only measurement process. In other words, we would like to obtain a probability density function (pdf) $p(\rho, \dot{\rho})$ that characterizes the PAR.We do so as follows. Firstly, notice that one can view the least squares solution for $(\alpha, \dot{\alpha}, \delta, \dot{\delta})$ from the short-arc, angles-only measurements as a mapping through which one can map the uncertainty in measurements to uncertainty in $(\alpha, \dot{\alpha}, \delta, \dot{\delta})$ at epoch. Let that pdf be denoted by $p(\alpha, \dot{\alpha}, \delta, \dot{\delta})$. Further assume that we have a probabilistic assessment of the distribution over the semi-major axis, a, and the eccentricity, e, with pdfs $p(a)$ and $p(e)$, respectively. We assume that the semi-major axis and the eccentricity are independent of each other and both from $(\alpha, \dot{\alpha}, \delta, \dot{\delta})$*. Distributions in a and e can be obtained from any known information and physics of the RSO population. In other words, the joint distribution in $(\alpha, \dot{\alpha}, \delta, \dot{\delta}, a, e)$ is given by:

$$p(\alpha, \dot{\alpha}, \delta, \dot{\delta}, a, e) = p(\alpha, \dot{\alpha}, \delta, \dot{\delta})p(a)p(e).$$

Using Eq. (7) and Eq. (11) one can map $p(\alpha, \dot{\alpha}, \delta, \dot{\delta}, a, e)$ to obtain $p(\rho, \dot{\rho})$.

Such an uncertainty map is impossible to achieve in closed-form, even when the measurement process is Gaussian. This is due to the nonlinearity present in Eq. (7) and Eq. (11). Therefore, in the present paper we will use the Monte Carlo method to obtain a particle representation of the uncertainty in $(\rho, \dot{\rho})$. Note that the mapping of Gaussian measurements to angles and angle-rates via the least squares mapping retains Gaussianity. In other words $p(\alpha, \dot{\alpha}, \delta, \dot{\delta})$ will be Gaussian under the assumption of a Gaussian measurement noise model. While in the next section we will assume that the measurement process is Gaussian, the Monte Carlo procedure described in the next section still holds as long as we can sample the pdf that describes the measurement process. If we are not able to sample the distribution, approximate MC methods, e.g., importance sampling, can be employed instead.

*In general, this is not true. The measurement process statistics are dependent on the orbital geometry, e.g., a and e.

4. A MONTE-CARLO REPRESENTATION OF THE PAR

Assuming that we know the observation process noise characteristics, Based on the discussion presented in the previous section, one can in principle map the uncertainty in the angles-only measurement process to the uncertainty in their rates given the

It is assumed that the sensor noise characteristics are known. For the sake of simplicity, we assume that the measurement noise is Gaussian with means $(\mu_i^{\alpha}, \mu_i^{\delta}$ and covariances $(\Sigma_i^{\alpha}, \Sigma_i^{\beta})$ for right ascension and declination, respectively, at time $t_i, i = 0, \ldots, n-1$. Following a batch least squares method [22], the measurements (α_i, δ_i), $i = 0, \ldots, n-1$, and their statistics can be mapped to a Gaussian distribution in $(\alpha_0, \dot{\alpha}_0, \delta_0, \dot{\delta}_0)$. Clearly, we can sample this distribution for the MC analysis. Let the particles in these variables be denoted by $\{(\alpha_0^{(j)}, \dot{\alpha}_0^{(j)}, \delta_0^{(j)}, \dot{\delta}_0^{(j)})\}$, $j = 1, \ldots, N$, where N is the chosen number of particles to represent the uncertainty cloud. Note that by our assumption that the semi-major axis and eccentricity are independent of the angles and the angle-rates, sampling of the the latter variables can be done by directly sampling from $p(\alpha_0, \dot{\alpha}_0, \delta_0, \dot{\delta}_0)$. Likewise, sample $p(a)$ directly to obtain semi-major axis particles $\{a^{(j)}\}$, and $p(e)$ to obtain eccentricity particles $\{e^{(j)}\}$, $j = 1, \ldots, N$. Notice that due to the statistical independence property, the ordering of the particles inside each of the three sets $\{(\alpha_0^{(j)}, \dot{\alpha}_0^{(j)}, \delta_0^{(j)}, \dot{\delta}_0^{(j)})\}$, $\{a^{(j)}\}$ and $\{e^{(j)}\}$ is irrelevant, but each particle from each set has to be uniquely and consistently matched with one from each of the other two sets to obtain joint particles $\{\mathcal{Y}^{(j)}\} = \{\alpha_0^{(j)}, \dot{\alpha}_0^{(j)}, \delta_0^{(j)}, \dot{\delta}_0^{(j)}, a^{(j)}, e^{(j)}\}$, $j = 1, \ldots, N$.

Next, each particle $\mathcal{Y}^{(j)}$ can now be inserted in Eq. (7) and Eq. (11) to obtain a particle $\mathcal{Z}^{(j)} = (\rho^{(j)}, \dot{\rho}^{(j)})$ in range, range-rate space. The resulting set of particles $\{\mathcal{Z}^{(j)}\} = \{(\rho^{(j)}, \dot{\rho}^{(j)})\}$ is then the desired particle cloud that represents the PAR.

5. CONVERTING THE PAR MC PARTICLE CLOUD INTO A PAR GMM

While an MC particle cloud is a faithful representation of the true uncertainty (within the bounds of the assumptions made in the procedure described above), it is difficult to perform many analytical computations (e.g., filtering using GMM techniques) with it in closed-form. This motivates the need to convert the PAR particle cloud into a PAR GMM, to name one important analytical model. This has been done previously by DeMars and Jah [12], where the CAR was modeled using a uniform distribution and a GMM approximation of the uniform distribution was proposed. Now that we have a non-uniform PAR, one needs to resort to more general methods for representing the PAR using a GMM. The standard procedure in the probabilistic inference literature is the EM method that can convert a sample (i.e., a particle cloud) into a GMM [19]. We will not describe the details of the method here. Instead we refer the reader to the algorithm in Ref. [20], which is a robust and versatile algorithm called the FJ-EM. The method allows for the user to specify a maximum number of GMM components and it selects the number of components that best represent the particle cloud. The user is also not required to choose a good initial guess of the components. In other words, the method does not require a careful initialization of the algorithm (other EM algorithms do require a very careful initialization.)

As an illustration, consider the 2000 particle cloud generated from the four component planar GMM with weights:

$$w_i = 0.25,\ i = 1, 2, 3, 4,$$

means:

$$\begin{aligned}
\boldsymbol{\mu}_1 &= [10.0\ 0.0]^{\mathrm{T}} \\
\boldsymbol{\mu}_2 &= [-10.0\ 0.0]^{\mathrm{T}} \\
\boldsymbol{\mu}_3 &= [0.0\ 10.0]^{\mathrm{T}} \\
\boldsymbol{\mu}_4 &= [0.0\ -10.0]^{\mathrm{T}}
\end{aligned}$$

and covariances:

$$\boldsymbol{\Sigma}_i = \begin{bmatrix} 2.0 & 0.0 \\ 0.0 & 2.0 \end{bmatrix},\ i = 1, 2, 3, 4.$$

The generated particle cloud was then fed into the FJ-EM algorithm and the following 5-component GMM initial guess was used for initializing the algorithm:

$$
\begin{aligned}
w_1^0 &= 0.1 \\
w_2^0 &= 0.4 \\
w_3^0 &= 0.2 \\
w_4^0 &= 0.2 \\
w_5^0 &= 0.1
\end{aligned}
$$

$$
\begin{aligned}
\boldsymbol{\mu}_1^0 &= [1.0\ 0.0]^{\mathrm{T}} \\
\boldsymbol{\mu}_2^0 &= [-1.0\ 0.0]^{\mathrm{T}} \\
\boldsymbol{\mu}_3^0 &= [0.0\ 1.0]^{\mathrm{T}} \\
\boldsymbol{\mu}_4^0 &= [-1.0\ -1.0]^{\mathrm{T}} \\
\boldsymbol{\mu}_5^0 &= [-5.0\ -5.0]^{\mathrm{T}}
\end{aligned}
$$

$$
\boldsymbol{\Sigma}_i^0 = \begin{bmatrix} 1.0 & 0.0 \\ 0.0 & 1.0 \end{bmatrix},\ i = 1, 2, 3, 4, 5.
$$

The algorithm resulted in the following set of GMM weights:

$$
\begin{aligned}
w_1^f &= 0.25 \\
w_2^f &= 0.24849 \\
w_3^f &= 0.26156 \\
w_4^f &= 0.23995 \\
w_5^f &= 0.0
\end{aligned}
$$

where we notice that one component has been eliminated. The final set of means were found to be

$$
\begin{aligned}
\boldsymbol{\mu}_1^f &= [9.96428\ 0.02116]^{\mathrm{T}} \\
\boldsymbol{\mu}_2^f &= [-9.87450\ -0.02471]^{\mathrm{T}} \\
\boldsymbol{\mu}_3^f &= [0.03449\ 10.06634]^{\mathrm{T}} \\
\boldsymbol{\mu}_4^f &= [0.04656\ -9.96678]^{\mathrm{T}}
\end{aligned}
$$

and the final set of covariances were found to be

$$
\begin{aligned}
\boldsymbol{\Sigma}_1^f &= \begin{bmatrix} 1.92951 & 0.02156 \\ 0.02156 & 1.92172 \end{bmatrix} \\
\boldsymbol{\Sigma}_2^f &= \begin{bmatrix} 2.10782 & -0.04989 \\ -0.04989 & 1.92587 \end{bmatrix} \\
\boldsymbol{\Sigma}_3^f &= \begin{bmatrix} 1.89439 & 0.05116 \\ 0.05116 & 2.35834 \end{bmatrix} \\
\boldsymbol{\Sigma}_4^f &= \begin{bmatrix} 1.99178 & 0.01623 \\ 0.01623 & 1.85653 \end{bmatrix}
\end{aligned}
$$

The resulting GMM is graphically shown in Figure 1 against the particles. Note that a component has a weight of zero (i.e., eliminated) resulting in an effective number of components of 4. While the true values of the weights, means and covariances were not recovered exactly, the error in these parameters is quite small. In the next section, we implement the FJ-EM algorithm in the PAR analysis, converting the particle cloud in the $\rho - \dot{\rho}$ space into a GMM representation of the PAR.

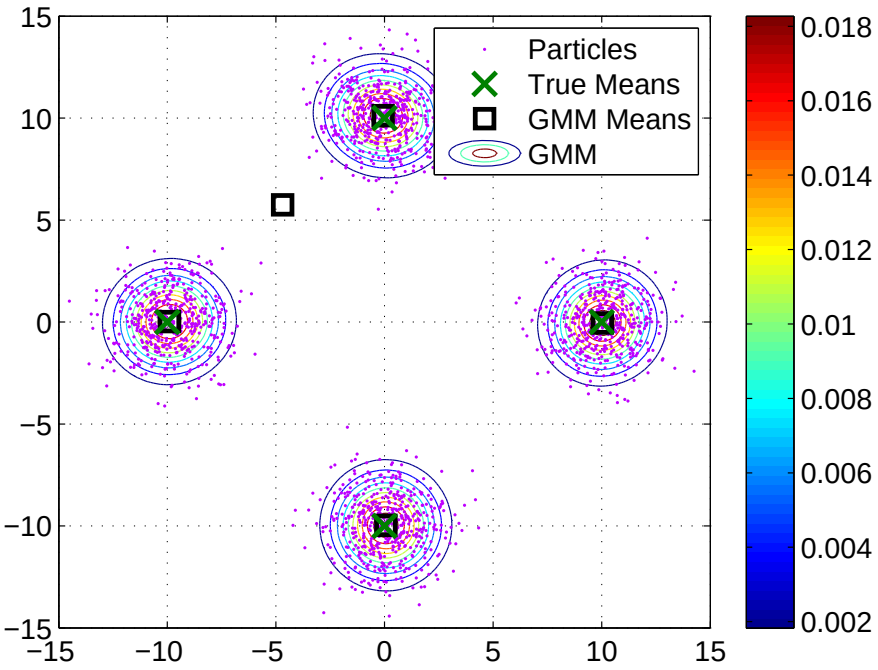

Fig. 1. An example showing the original means (equally weighted) that generated the shown particle cloud. The cloud was then fed into the FJ-EM algorithm that generated the GMM approximation shown. The FJ-EM algorithm was able to very accurately reconstruct the true GMM that generated the particle cloud.

6. SIMULATION RESULTS

In this section we provide a numerical example that demonstrates the above ideas. We consider an orbit with the orbital element values shown in Table 1 at the initial simulation time. Using the Socorro, NM, ground sensor, 9 right ascension and declination observations were collected at the rate of one observation every 20 seconds. The measurement noise is assumed to be Gaussian with an angular standard deviation of 2 arcsec for both right ascension and declination.

Table 1. Orbital Elements of the True Orbit

Orbital Element	Value
Semimajor Axis (km)	26 571.
Eccentricity	0.2
Inclination (deg)	55.0
Perigee (deg)	-120.0
Right Ascension of the Ascending Node (deg)	-13.24
Initial True Anomaly (deg)	110.0

The 9 measurements and their statistics are then used to obtain the (Gaussian) statistics for the attributable vector at epoch using the method of Maruskin et al. [7]. Because each of the measurement statistics is assumed Gaussian and the batch least-squares solution preserves Gaussianity, the attributable vector was found to have the following mean:

$$\begin{bmatrix} \mu_\alpha \\ \mu_{\dot\alpha} \\ \mu_\delta \\ \mu_{\dot\delta} \end{bmatrix} = \begin{bmatrix} -0.32184 \\ 3.37094 \\ 1.33430\text{e}^{-4} \\ 8.08795\text{e}^{-5} \end{bmatrix}$$

and covariance:

$$\begin{bmatrix} 6.21086\mathrm{e}^{-11} & -1.45300\mathrm{e}^{-12} & 0.0 & 0.0 \\ -1.45300\mathrm{e}^{-12} & 5.27577\mathrm{e}^{-14} & 0.0 & 0.0 \\ 0.0 & 0.0 & 6.21086\mathrm{e}^{-11} & -1.45300\mathrm{e}^{-12} \\ 0.0 & 0.0 & -1.45300\mathrm{e}^{-12} & 5.27577\mathrm{e}^{-14} \end{bmatrix}.$$

The reason the covariance matrix has a block form is that the right ascension and declination angular measurements are independent. Semi-major axis is assumed be uniformly distributed between 10,000 km and 50,000 km. Eccentricity is assumed to be uniformly distributed between 0.0 and 0.4.

For each particle $\mathcal{Y}^{(j)}$, Eq. (7) can be used to construct a curve in the $\rho - \dot{\rho}$ space corresponding to the sampled $a^{(j)}$ value. Repeating for all particles $\mathcal{Y}^{(j)}$ we obtain a "cloud" of semi-major axis curves (which we shall call the "a-curves"). Figure 2 shows the cloud generated from a set of 500 particles $\mathcal{Y}^{(j)}$. Likewise, Eq. (11) can be used to construct a cloud of $e^{(j)}$ curves (which we shall call the "e-curves"), shown in Figure 3. Recall that there is exactly one a-curve that corresponds to one e-curve. The intersection (if an intersection exists) of these two sets of curves results in the particle cloud in the $\rho - \dot{\rho}$ space (we do not plot the particles, but show the curves and their intersections in Figure 4).

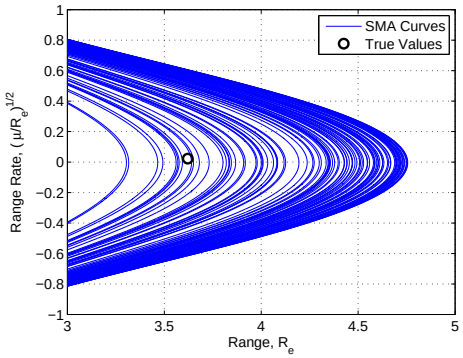

Fig. 2. The "cloud" of a-curves.

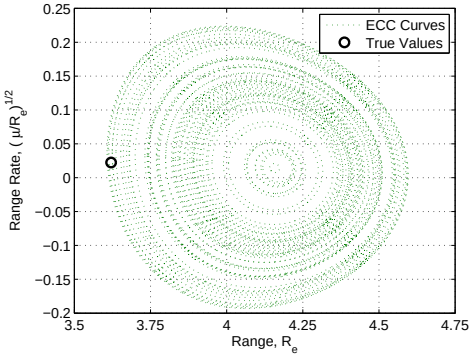

Fig. 3. The "cloud" of e-curves.

We selected a relatively small number of particles above to demonstrate the non-uniformity of the a- and e-curves (otherwise, the plot is too dense to be able to see the distribution of the curves). Using a sample of 4000 particles instead of 500 we get the $\rho - \dot{\rho}$ particle cloud sown in Figure 5. The figure also shows the GMM approximation of the particle cloud generated from the FJ-EM algorithm. For the initial GMM we grid the $\rho - \dot{\rho}$ space into a set of 10 ten grid points along each direction, for a total of 100 grid points). This grid defines the means of the initial GMM. All components had the same weight of $1/100 = 0.01$ and all have the same covariances with a standard deviation of one-tenth of an earth radius in the ρ direction and 200 meter per second in the $\dot{\rho}$ direction. The generated GMM had

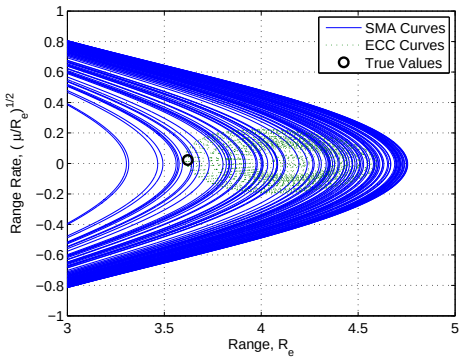

Fig. 4. The "cloud" of a- and e-curves overlaid on top of each other.

a total of 38 non-zero components (using a threshold of 0.0001 for the weights). As can be seen, the GMM seems to reflect the cloud rather faithfully. This GMM can now be used along the lines suggested by DeMars and Jah [12] in a Bayesian filtering scheme.

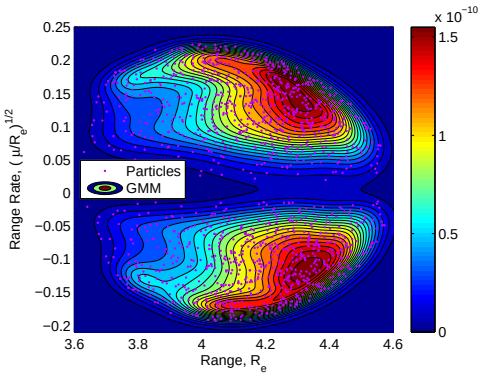

Fig. 5. The particle "cloud" in $\rho - \dot{\rho}$ space at its FJ-EM-based GMM approximation.

7. CONCLUSION

In this paper we used a Monte Carlo approach to show how to construct a probabilistic admissible region in $\rho - \dot{\rho}$ space. The PAR, as shown, is clearly non-uniform. We also proposed to use the FJ-EM algorithm to convert the particle cloud into a GMM representation of the PAR. This GMM can then be used to initialize a Bayesian filter. In this paper we addressed the situation where only two constraints exist (semi-major axis and eccentricity). Current work focuses on allowing additional constraints, such as a minimum constraint on perigee.

REFERENCES

[1] A. Milani, G. F. Gronchi, M. d. Michieli Vitturi, and Z. Knežević, "Orbit Determination with Very Short Arcs: I. Admissible Regions," *Celestial Mechanics and Dynamical Astronomy*, Vol. 90, September 2004, pp. 59–87.

[2] A. Milani and Z. Knežević, "From Astrometry to Celestial Mechanics: Orbit Determination with Very Short Arcs," *Celestial Mechanics and Dynamical Astronomy*, Vol. 92, No. 1–3, 2005, pp. 1–18.

[3] G. Tommei, A. Milani, and A. Rossi, "Orbit Determination of Space Debris: Admissibile Regions," *Celestial Mechanics and Dynamical Astronomy*, Vol. 97, 2007, pp. 289–304.

[4] G. Tommei, A. Milani, D. Farnocchia, and A. Rossi, "Correlation of Space Debris Observations by the Virtual Debris Algorithm," *Proccedings of the 5th European Conference on Space Debris*, European Space Operations Center, Darmstadt, Germany, March 30–April 2 2009.

[5] A. Milani, G. Tommei, D. Farnocchia, A. Rossi, T. Schildknecht, and R. Jehn, "Correlation and Orbit Determination of Space Objects based on Sparse Optical Data," *Monthly Notices of the Royal Astronomical Society*, Vol. 417, No. 3, 2011, pp. 2094–2103.

[6] D. Farnocchia, G. Tommei, A. Milani, and A. Rossi, "Innovative Methods of Correlation and Orbit Determination for Space Debris," *Celestial Mechanics and Dynamical Astronomy*, Vol. 107, 2010, pp. 169–185.

[7] J. M. Maruskin, D. J. Scheeres, and K. T. Alfriend, "Correlation of Optical Observations of Objects in Earth Orbit," *Journal of Guidance, Control, and Dynamics*, Vol. 32, January–February 2009, pp. 194–209.

[8] K. Fujimoto, J. M. Maruskin, and D. J. Scheeres, "Circular and Zero-Inclination Solutions for Optical Observations of Earth-Orbiting Objects," *Celestial Mechanics and Dynamical Astronomy*, Vol. 106, 2010, pp. 157–182.

[9] K. Fujimoto and D. J. Scheeres, "Correlation of Optical Observations of Earth-Orbiting Objects and Initial Orbit Determination," *Journal of Guidance, Control, and Dynamics*, Vol. 35, January–February 2012, pp. 208–221.

[10] G. F. Gronchi, L. Dimare, and A. Milani, "Orbit Determination with the Two-Body Integrals," *Celestial Mechanics and Dynamical Astronomy*, Vol. 107, 2010, pp. 299–318.

[11] K. J. DeMars, M. K. Jah, and P. W. Schumacher, Jr., "Initial Orbit Determination using Short-Arc Angle and Angle Rate Data," *IEEE Transactions on Aerospace and Electronic Systems*, Vol. 43, July 2012, pp. 2628–2637.

[12] K. J. DeMars and M. K. Jah, "Probabilistic Initial Orbit Determination Using Gaussian Mixture Models," *Journal of Guidance, Control, and Dynamics*, Vol. 36, September–October 2013, pp. 1324–1335.

[13] J. A. Siminski, H. Fiedler, and T. Schildknecht, "Track Association Performance of the Best Hypotheses Search Method," *Proccedings of the 6th European Conference on Space Debris*, European Space Operations Center, Darmstadt, Germany, April 22–25 2013.

[14] J. A. Siminski, O. Montenbruck, H. Fiedler, and M. Weigel, "Best Hypothesis Search on Iso-Energy-Grid for Initial Orbit Determination and Track Association," *Advances in the Astronautical Sciences*, Vol. 148, 2013, pp. 605–617. (Proceedings of the 23rd AAS/AIAA Space Flight Mechanics Meeting, Kauai, HI, February 10–14 2013, Paper 13-239).

[15] P. W. Schumacher, Jr., M. P. Wilkins, and C. W. T. Roscoe, "Parallel Algorithm for Track Initiation for Optical Space Surveillance," *Proccedings of the 6th European Conference on Space Debris*, European Space Operations Center, Darmstadt, Germany, April 22–25 2013.

[16] C. W. T. Roscoe, P. W. Schumacher, Jr., and M. P. Wilkins, "Parallel Track Initiation for Optical Space Surveillance using Range and Range-Rate Bounds," *Advances in the Astronautical Sciences*, Vol. 150, 2014, pp. 989–1008. (Proceedings of the AAS/AIAA Astrodynamics Specialist Conference, Hilton Head, SC, August 11–15 2013, Paper AAS 13-767).

[17] I. I. Hussein, C. W. T. Roscoe, M. P. Wilkins, and P. W. Schumacher, Jr., "Probabilistic Admissibility in Angles-Only Initial Orbit Determination," *Proceedings of the 24th International Symposium on Space Flight Dynamics*, Laurel, MD, May 5–9 2014.

[18] J. L. Worthy III and M. J. Holzinger, "Incorporating Uncertainty in Admissibile Regions for Uncorrelated Detections," *Proceedings of the AIAA/AAS Astrodynamics Specialist Conference*, San Diego, CA, August 4–7 2014.

[19] A. P. Dempster, N. M. Laird, and D. B. Rubin, "Maximum Likelihood from Incomplete Data via the EM Algorithm," *Journal of the Royal Statistical Society, Series B*, Vol. 39, 1977, pp. 1–38. 1.

[20] M. A. T. Figueiredo and A. K. Jain, "Unsupervised Learning of Finite Mixture Models," *IEEE Transactions on Pattern Analysis and Machine Intelligence*, Vol. 24, 2002, pp. 381–396. 3.

[21] A. E. Roy, *Orbital Motion*. Taylor and Francis Group, 1988.

[22] J. L. Crassidis and J. L. Junkins, *Optimal Estimation of Dynamic Systems*. Boca Raton, FL: Chapman & Hall/CRC Applied Mathematics and Nonlinear Science Series, 2004.